Phase Field Crystal Methods for Bilayer Graphene

Kai Liu

College of education for the future, Beijing Normal University, at Zhuhai, China.

liuk@bnu.edu.cn

Abstract. Bilayer graphene has been a subject of intense study in recent years. We extend a structural phase field crystal method to include an external potential based on the generalized stacking-fault energy that accounts for the effect from a bottom layer of graphene. Both of the favored stacking variants are found with randomly generated initial phase fields. Using the width of the boundaries between different stacking variants as a function of the interactions between the two layers, we quantify the exact strength of the external potential by comparing the phase field crystal simulations with the results from atomistic simulation. We simulate a circular grain of one stacking phase enclosed by the other and find that, depending on the initial phase field, the center domain may shrink to form a uniform stacking phase, or may evolve to a relaxed state of a hexagon region or a triangular region that at each vertex the graphene structure is defected.

Keywords: graphene; phase field method; bilayer structure; stacking energy.

1. Introduction

Graphene, a single layer of carbon atoms tightly bound in a hexagonal honeycomb lattice, is one of the most exciting new two-dimensional materials discovered. Bilayer graphene, consists of two coupled single layers of honeycomb crystal structure of carbon atoms, has attracted a great deal of attention because it can exist with a variety of stacking arrangement with intriguing electronic properties [1,2,3,4,5].

Computational modeling can serve as a route for theoretically understanding the difficult-to-measure properties of graphene. On the continuum scale, the phase field crystal (PFC) modeling approach describes the thermodynamic and dynamic of phase transformation through an atomically varying order parameter field that is loosely connected to the atomic density field. The original PFC model was predominately used for the study of 2D triangular and three-dimensional (3D) crystal symmetries [6, 7]. It is a promising and widely used approach for modeling many microstructure phenomena. Recently, PFC has been used to study how anisotropic diffusion of carbon on a surface can yield the formation of the dendritic graphene structure [8]. By including a rotationally invariant three-point correlation function for the excess free energy, a structural PFC model was set up to address both the atomically varying defect and microstructures of graphene and its nucleation and diffusional growth kinetics from a disordered state on a surface [9].

In this paper, we build a new PFC model for bilayer graphene by extending the structural phase field crystal method in [9]. Following [9], we use a structural PFC model that includes both two-point correlation kernels and three-point correlations in the nonlocal part of the free energy. In order to model the effect of a second layer of graphene on the layer we are modeling we introduce a local interaction between the order parameter density and an external potential. We will refer to the external potential as the bottom-layer potential. The most relevant physical picture would be when the bottom graphene layer is completely fixed after deposition on a substrate, and the layer we are modeling is deposited on it. The bottom-layer potential is chosen based on first-principles calculations of the generalized stacking fault energy (GSFE) in bilayer graphene from reference [12]. The GSFE is the energy landscape seen when one layer of graphene is moved laterally and uniformly with respect to the other layer. The fitted form of the GSFE in reference [12] is such that a bottom-layer potential of the same form (but different coefficients) applied in an atomistic calculation would reproduce that GSFE exactly. We have used that bottom-layer potential in the PFC model, but multiplied by an arbitrary parameter, which we fit to molecular dynamics (MD)

simulations. The MD model is validated by comparison with experimental results, as discussed later.

In the numerical simulations, we first test the growth of graphene phases without the bottom-layer potential by choosing parameters corresponding to the solid region of the phase field, i.e. ensuring the periodicity for each side of the rectangular domain and initializing the system with Gaussian noise. The results agree with [9]. We then add bottom layer potential and again start with Gaussian noise and generate both the AB and BA stacking, where AB and BA stacking have one of the first layer's sublattice atoms (A or B) directly on top of its opposite sublattice atom (B or A) in the second layer, called AB or BA stacking, respectively, or collectively called Bernal stacking [13].

Next we test the case of a long narrow ribbon domain. The initial condition consists of 4 parts, continuous AB and BA region each of nearly 50% of the entire domain respectively and two narrow transition between them each is set to be a constant with small Gaussian perturbation. We find four transition types, depending on the angle

between the transition region and the shifting direction, 0^◦ ,30^◦ ,60^◦ , and 90^◦ . By comparing with the simulation results from atomistic methods, we quantify the strength of the bottom layer potential by the width of the transition region for each type of transition.

We then test the case of a circular AB vs BA stacking. With constant transition region, the center part (even a relatively small one) may evolve to a triangular or hexagonal shape with at least one 5-7 defective ring on each vertex. On the other hand, with uniformly smooth transition from AB to BA, the area of the center part will shrink at a constant speed (even for a relatively large disk).

The simulations are numerically expensive that it takes a long time, i.e. 3-7 days, to reach a steady solidification. In order to solve the system in a large domain efficiently, we use a CUDA C/C++ programming on Nvidia Quadro GV100, which runs about 2 orders of magnitude faster than the normal CPU.

2. Modeling and Method

2.1 Modeling

We incorporated a generalized stacking-fault energy into the structural PFC model [9,12]. Let ρ describe the spatial phase density of carbon atoms. A dimensionless density field is then defined as $\psi = (\rho - \bar{\rho})/\bar{\rho}$, where $\bar{\rho}$ is the mean value of ρ. The free energy of a crystallizing system reads as

$$F_{\text{total}} = F_{\text{id}}(\psi) + F_{\text{ex,2}}(\psi) + F_{\text{ex,3}}(\psi) + F_{\text{GSFE}}(\mathbf{x}) \tag{1}$$

where F_{id} is the ideal free energy, $F_{\text{ex,2}}$ the two-point interactions, $F_{\text{ex,3}}$ the three-point correlations [9], and $F_{\text{GSFE}}(\text{x})$ the generalized stacking-fault energy of graphene [12]. F_{id} is given by

$$F_{\text{id}} = \int d\mathbf{x}\left\{\frac{\psi^2}{2} - \eta\frac{\psi^3}{6} + \chi\frac{\psi^4}{12}\right\} \tag{2}$$

where η and χ are dimensionless parameters and we simply set $\eta = \chi = 1$. The two-point interactions is given by

$$F_{\text{ex,2}} = -\frac{1}{2}\int \psi(\mathbf{x}) \int C_2(\mathbf{x} - \mathbf{x}')\psi(\mathbf{x}')d\mathbf{x}'d\mathbf{x} \tag{3}$$

Here C_2 is the two-point correlation function defined as [9]

$$C_2(\boldsymbol{x}) = -\frac{R}{\pi r_0^2} circ\left(\frac{r}{r_0}\right), \tag{4}$$

where r_0 sets the cutoff for the repulsive term, R sets the magnitude of the repulsion, and

$$circ(r) = \begin{cases} 1, & r \le 1, \\ 0, & r > 1. \end{cases} \tag{5}$$

The three-point correlations is governed by

$$F_{\text{ex},3} = -\frac{1}{3}\int \psi(\mathbf{x}) \int C_3(\mathbf{x}-\mathbf{x}', \mathbf{x}-\mathbf{x}'')\psi(\mathbf{x}')\psi(\mathbf{x}'')d\mathbf{x}'d\mathbf{x}''d\mathbf{x} \tag{6}$$

Here

$$C_3(\mathbf{x}-\mathbf{x}', \mathbf{x}-\mathbf{x}'') = \sum_i C_s^{(i)}(\mathbf{x}-\mathbf{x}')C_s^{(i)}(\mathbf{x}-\mathbf{x}'') \tag{7}$$

where $C_s^{(i)}$ in polar coordinate reads as [9]

$$C_s^{(1)}(r,\theta) = C_r(r)\cos(m\theta), \quad C_s^{(2)}(r,\theta) = C_r(r)\sin(m\theta), \qquad C_r(r) = \frac{X}{2\pi a_0}\delta(r-a_0) \tag{8}$$

Here X is a parameter defining the strength of the interaction, a_0 corresponds to the lattice spacing and $r_0/a_0 = 1.22604$, and $m = 3$ defines bond order of the crystal phase. For the graphene system, $R = 6$ and $X^{-1} = 0.4$ [9].

The generalized stacking-fault energy reads as

$$\begin{aligned}
\lambda F_{\text{GSFE}} = c_0 &+ c_1\left[\cos\frac{2\pi}{a_s}\left(x+\frac{y}{\sqrt{3}}\right) + \cos\frac{2\pi}{a_s}\left(x-\frac{y}{\sqrt{3}}\right) + \cos\frac{4\pi y}{\sqrt{3}a_s}\right] \\
&+ c_2\left[\cos\frac{2\pi}{a_s}(x+\sqrt{3}y) + \cos\frac{2\pi}{a_s}(x-\sqrt{3}y) + \cos\frac{4\pi x}{a_s}\right] \\
&+ c_3\left[\cos\frac{2\pi}{a_s}\left(2x+\frac{2y}{\sqrt{3}}\right) + \cos\frac{2\pi}{a_s}\left(2x-\frac{2y}{\sqrt{3}}\right) + \cos\frac{8\pi y}{\sqrt{3}a_s}\right], \\
&+ c_4\left[\sin\frac{2\pi}{a_s}\left(x-\frac{y}{\sqrt{3}}\right) - \sin\frac{2\pi}{a_s}\left(x+\frac{y}{\sqrt{3}}\right) + \sin\frac{4\pi y}{\sqrt{3}a_s}\right] \\
&+ c_5\left[\sin\frac{2\pi}{a_s}\left(2x-\frac{2y}{\sqrt{3}}\right) - \sin\frac{2\pi}{a_s}\left(2x+\frac{2y}{\sqrt{3}}\right) + \sin\frac{8\pi y}{\sqrt{3}a_s}\right]
\end{aligned} \tag{9}$$

where a_s is the distance between two nearby minimum points, i.e., two nearby holes on the bottom layer of graphene. $c_0 = 21.336, c_1 = 12.254, c_2 = -1.128, c_3 = -0.286, c_4 = \sqrt{3}c_1$, and $c_5 = -\sqrt{3}c_3$ [12]. Note that λ is a parameter measuring the strength of the GSFE. The GSFE substrate potential when $\lambda = 1$ is shown by Fig. 1, where the maximum and the minimum points are the location of carbon atoms and center of the holes on the bottom layer correspondingly.

Given $a_s = \sqrt{3}d_c$, where d_c is the distance between two nearby atom centers. In the structural PFC model [9], $d_c = \frac{\sqrt{3}}{2\pi}a_0$, therefore, $a_s = 3a_0/2\pi$. Finally, the evolution of the density n, which is a conserved order parameter, is governed by

$$\frac{\partial\psi}{\partial t} = M_\psi\nabla^2\left(\frac{\delta F_{\text{total}}}{\delta\psi}\right) \tag{10}$$

where M_ψ is an effective mobility that scales of the diffusional dynamics of ψ and we set $M_\psi = 1$ for convenience.

2.2 Numerical Methods

We use a discrete Fourier transform (DFT) method to solve Eq. (8). The two points correlation structure $F_{ex,2}$ is computed by [9]

$$\frac{\partial F_{ex,2}}{\partial \psi} = -\int C_2(\mathbf{x}-\mathbf{x}')\psi(\mathbf{x}')d\mathbf{x}' \equiv -C_2 * \psi \tag{11}$$

where $*$ is a convolution in the domain, and in the reciprocal space

$$\hat{C}_2(\mathbf{k}) = -2RJ_1(r_0k)/r_0k, k = \sqrt{k_1^2+k_2^2} \tag{12}$$

where J_m are the Bessel functions of the first kind, and k_1, k_2 are the modes in the 2D reciprocal space. The three points correlation structure $C_3(r-r', r-r'')$ is separated to

$$C_3(\mathbf{r}-\mathbf{r}', \mathbf{r}-\mathbf{r}'') = \sum_i C_s^{(i)}(\mathbf{r}-\mathbf{r}')C_s^{(i)}(\mathbf{r}-\mathbf{r}'') \tag{13}$$

The $F_{ex,3}$ is then computed as [9]

$$\frac{\partial F_{ex,3}}{\partial \psi} = -\frac{1}{3}\left\{\left[C_s^{(i)} * \psi\right]^2 + 2(-1)^m C_s^{(i)} * \left[\psi \cdot \left(C_s^{(i)} * \psi\right)\right]\right\}, \tag{14}$$

where $\hat{C}_s^{(1)}(k,\theta_k) = Xi^m \cos(m\theta_k)J_m(ka_0)$, $\hat{C}_s^{(2)}(k,\theta_k) = Xi^m \sin(m\theta_k)J_m(ka_0)$, and $k = \sqrt{k_1^2+k_2^2}, \theta_k = \arctan\left(\frac{k_2}{k_1}\right)$.

To incorporate the F_{GSFE}, we need to ensure $F_{GSFE}(x)$ is periodic for each side, i.e., the aspect ratio of the rectangular domain must be $n_1:\sqrt{3}n_2$, where n_1 and n_2 are positive integers. For rectangular domain $L \times \sqrt{3}L$, by setting $k = \sqrt{k_1^2 + 3 \times k_2^2}$, $\theta_k = \arctan\left(\frac{\sqrt{3}\times k_2}{k_1}\right)$, C_2 and $C_s^{(i)}$ functions are then of circular shapes. Note that the Laplacian operator also needs to be scaled to ensure that the diffusion is invariant of direction.

Since we solve the system in a large domain, e.g., $N_X \times N_Y = 1024 \times (32 \times 1024)$. FFT is extremely efficient by GPU parallelization, since the bandwidth of the memory is the bottleneck of the performance for FFT algorithm. Here we use a CUDA C/C++ parallel programming to accelerate our algorithm, which runs about 2 orders of magnitude faster than normal CPU version. The Nvidia Tesla K40 is used, whose memory bandwidth is 288 GB/s.

3. Results

3.1 Preliminary test of the model.

We set the initial phase diagram $\psi(x,0) = 0.3 + \mathcal{Z}(x)$, where $\mathcal{Z}(x)$ is a spacial uncorrelated scaler field of Gaussian noise with mean 0 and standard deviation 0.001. When $F_{GSFE} = 0$, i.e., $\lambda = \infty$, the graphene evolves to a defected structure that agree with [9]. Then we set $\lambda = 500$ and the initial phase diagram $\psi(x,0) = 0.3 + \mathcal{Z}(x)$ that the graphene evolves to a neat structure and it takes shorter time to reach such an equilibrium.

Next we simulate a group of samples by setting $\lambda = 500$ and initial phase diagram again $\psi(x,0) = 0.3 + \mathcal{Z}(x)$ with different random seeds. We find both AB and BA stacking phases [13],

as shown in Fig. 1. In the left picture of Fig. 1, we plot the bottom layer that the carbon atoms are classified into two categories with one group colored by lighter green and the other by darker green. One lighter green atom is near to three darker atoms and vice versa. In Fig. 1(b), we plot AB stacking order where the upper layer atoms locate above the darker green atoms and the center of the hexagons, comparing with BA stacking, plotted in Fig. 1(c), where the upper layer atoms locate above the lighter green atoms and center of hexagons.

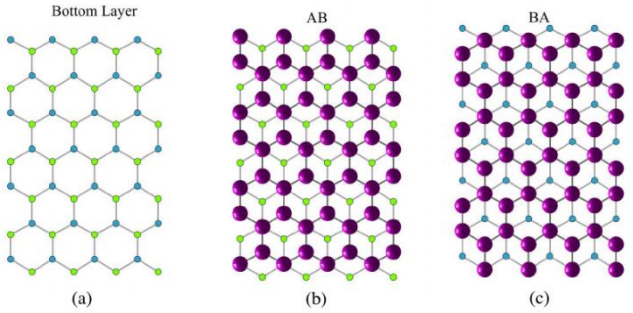

Fig. 1 (a) Bottom layer atoms are classified into 2 groups, one denoted by lighter green and the other darker green. (b) Phase distribution for AB pattern when $\lambda = 500$. (c) Phase distribution for BA pattern.

3.2 The transition between the AB and BA stacking order

Given a long ribbon of bilayer graphene, where AB phase and BA phase are of equal length, we investigate the transition between them. The initial conditions is a static setup where there are 4 parallel stripes $X - Y - Z - W$. X represents the stacking order AB, Z represents the stacking order BA, and Y, W are disordered. The X and Z region grows as the dynamics start and two interfaces will be created between them. We find that the interface depends on the constant λ, i.e. the strength of the GSFE. This allows one to tuning λ by comparing the width to the one from atomistic simulations and experimental results. There are 2 boundaries: one from AB to BA and the other from BA to AB.

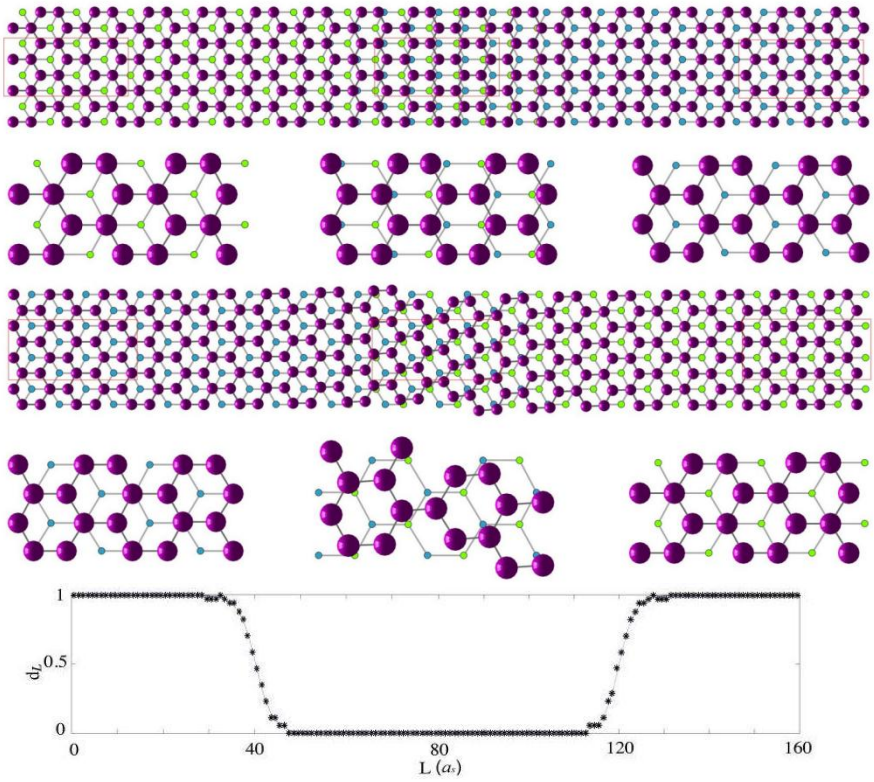

Fig. 2. Fitting of the transition width by $d = \arctan(\exp(\pi L/W))$ for the left region and the right region

We then compute the thickness of the transition region. Define a parameter $\mathrm{d} = \mathrm{mean}\left(\mathrm{d}_{\mathrm{L_i}}\right)$ that measures the distortion between substrate potential $\mathrm{F_{GSFE}(x)}$ and the graphene field $\psi(\mathrm{x})$, where $\mathrm{d_L}$ is the nondimensionalized $\mathrm{x-y}$ plane distance between the center of one group of atoms on the bottom layer and the nearest atom centers on the top layer at $\mathrm{x_i}$. We set $\mathrm{d} = 1$ for AB pattern and $\mathrm{d} = 0$ for BA pattern. The data is then fitted by the function $\mathrm{d} = \arctan\left(\exp\left(\frac{\pi \mathrm{L}}{\mathrm{W}}\right)\right)$, where W is a fitting parameter stands for the thickness of the transition region. The real width (full width at half maximum) is a little smaller, nevertheless we use W for convenience. As shown in Fig. 2, $\mathrm{W_{90}} > \mathrm{W_{30}}$ given the same $\mathrm{F_{GSFE}(x)}$, which agrees with previous results [13].

We then quantify the coefficient λ. Start from $\psi_{\mathrm{o}}(\mathrm{X})$, we use bisection method to pin down the value of λ, i.e. $\lambda_0 = 10000, \lambda_1 = 5000, \lambda_2 = 7500, \ldots$ We compare the value of $\mathrm{W_\lambda^0}$ and $\mathrm{W_\lambda^{90}}$ with the atomistic results, that if the relative difference between the PFC results and atomistic simulation results are smaller than 5% for all the cases, we accept that λ. We did not use the value of $\mathrm{W_\lambda^{\pm 30}}$ or $\mathrm{W_\lambda^{\pm 60}}$ since the domain is a narrow ribbon that the exact direction of the transition region is not quite precise for those two cases. By this procedure, we found that $\lambda = 7500$ is a proper value, considering all the three cases $\mathrm{W_0}$ and $\mathrm{W_{\pm 90}}$, as shown in Fig. 3. Note that for a single value of λ our PFC results agree reasonably well with atomistic simulations.

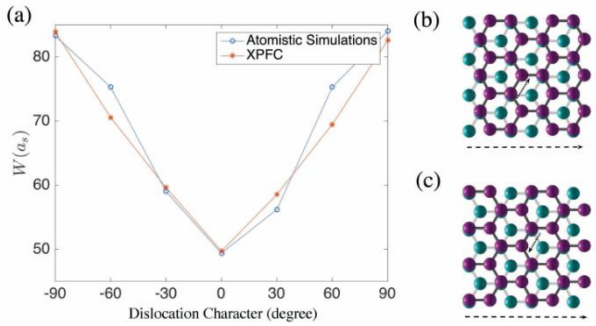

Fig. 3. (a) the relation between the dislocation direction and W when $\lambda = 7500$. The AB to BA transition enforce the atoms on the top layer (pink balls) to move along the dashed arrow. Therefore, case (b) is elongation $(+)$, and case (c) is compression (-).

3.3 A circular shape transition between AB and BA

Another good setup to investigated into is the dynamics of a (circular) disk shaped grain of one stacking order, with the rest of the cell the other stacking order. One expects the circular grain to shrink and the final configuration to be a uniform stacking order. But that is not what observed in the experiments. The initial phase diagram is created following Fig. 4. Here we set $\mathrm{a} = 8\mathrm{a_s}, \mathrm{b} = 16\mathrm{a_s}$, and $\mathrm{c} = 64\mathrm{a_s}$.

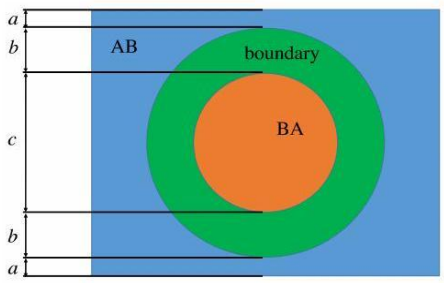

Fig. 4. A script of the initial phase diagram for the circular shape.

The simulation reaches an equilibrium where the BA stacking order region is similar to a hexagon, as shown in Fig. 5 (a). The outer region is of AB stacking order, and interior region is of BA stacking order. The direction of the hexagon region is in consistent with the orientation of the atomic alignment on the bottom layer. Note that the small regions on the six vertices of the large hexagon is obviously different from nearby parts, and those verticescan be classified into two categories.

In Fig. 5 (b), we plot the phase diagram of the zoomed in patch whose position is denoted by the red dashed rectangle in Fig. 5 (a). This patch includes 2 nearby vertices of the large hexagon. In Fig. 5 (c) and (d), we zoom in again and plot in detail of the phase diagram, with black and red circles denoting the atoms on the bottom layer. By careful scrutiny, we find that in the left sub-patch there are well-structured BA stacking parts on the bottom-right corner and in the right sub-patch there are well-structured AB stacking parts on the top, which agrees with Fig. 5 (a). Also note that in Fig. 5 (c) and (d), there are defective regions, and they will not disappear. This partially explains why the center region will not shrink to zero.

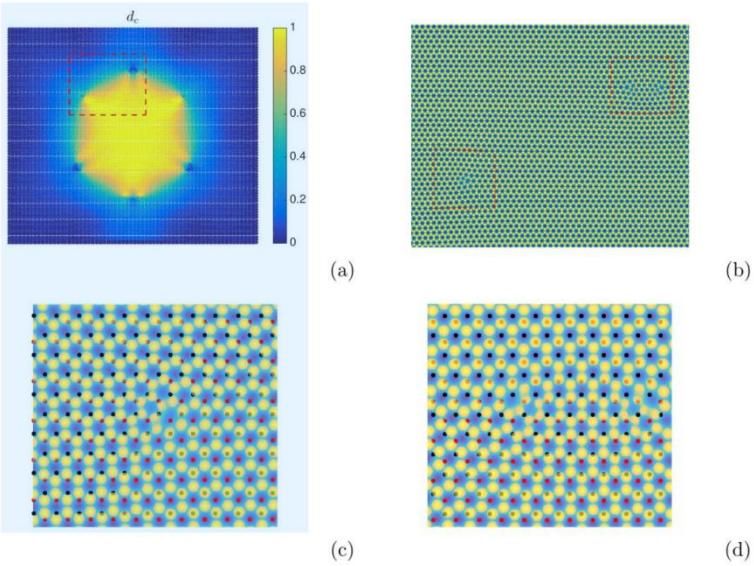

Fig. 5. (a) The whole domain for the final equilibrium state. (b) The phase diagram of the zoomed in patch from (a). (c) Phase diagram for the left sub-patch with black and red circles denoting the atoms on the bottom layer. (d) Phase diagram for the right sub-patch with black and red circles denoting the atoms on the bottom layer.

4. Conclusion

We build a new PFC model to include generalized stacking-fault energy that account for the effect of a bottom layer of graphene. In order to ensure the periodicity, we scale the parameters to extend the model to fit a rectangular domain of $n_1 \times \sqrt{3}n_2$, where n_1, n_2 are integers. A special simulation strategy is used to attain computational efficiency, even if an efficient GPU parallelization is implemented.

We first test the algorithm by setting $\lambda = \infty$, i.e. no substrate potential, and $\lambda = 500$, which is more than 10 times of the appropriate substate potential. We find both AB and BA stacking phases, and a defective phase state will evolve to an ordered state quickly by adding the substrate potential. Those simulations agree with previous numerical works and experiments qualitatively.

We then quantity the scaling coefficient λ. Using the width of the transition region between AB and BA stacking order and a function of the strength of the substrate potential F_{GSFE}, we pin down the value that when $\lambda = 7500$ the PFC results agree with the atomistic results for all the four transition angles, $0°, 30°, 60°, 90°$, elongated or compressed.

Unlike our intuitive expectation, the circular grain of one stacking order enclosed by the other stacking order, will not shrink to a uniform stacking order. But the center disk will evolved into a hexagon with six vertices specifically defected.

A potential future work is to use the phase diagram $\psi(x)$, as the FGSF E. Then the effect of the top layer onto the bottom layer could be defined in a similar way. By doing so, both layers could evolve, and the compression-elongation difference might disappear.

References

[1] Oostinga, J, Heersche, H., LIU, Xinglan, Morpurgo, A., Vandersypen, L. Gate-induced insulating state in bilayer graphene devices, Nature Materials, 2008, 7: 151-157.

[2] B. Butz, C. Dolle, F. Niekiel, K. Weber, D. Waldmann, H. B. Weber, B. Meyer, E. Spiecker. Dislocations in bilayer graphene, Nature, 2014, 505(7484): 533-537.

[3] CAO Yu, V. Fatemi, S. Fang, K. Watanabe, T. Taniguchi, E. Kaxiras, P. Jarillo-Herrero. Unconventional superconductivity in magic-angle graphene superlattices, Nature, 2018, 556(7669): 43-50.

[4] T. Ohta, A. Bostwick, T. Seyller, K. Horn, and E. Rotenberg. Controlling the electronic structure of bilayer graphene, Science, 2006, 313(5789): 951-954.

[5] M. Yankowitz, CHEN Shaowen, H. Polshyn, ZHANG Yuxuan, K. Watanabe, T. Taniguchi, D. Graf, A. F. Young, C. R. Dean. Tuning superconductivity in twisted bilayer graphene, Science, 2019, 363(6431): 1059-1064.

[6] K. Elder, M. Grant. Modeling elastic and plastic deformations in nonequilibrium processing using phase field crystals, Physical Review E, 2004, 70(5): 051605.

[7] K. Elder, M. Katakowski, M. Haataja, M. Grant. Modeling elasticity in crystal growth, Physical review letters, 2002, 88(24): 245701.

[8] E. Meca, J. Lowengrub, H. Kim, C. Mattevi, V. B. Shenoy. Epitaxial graphene growth and shape dynamics on copper: phase-field modeling and experiments, Nano letters, 2013, 13(11):5692-5697.

[9] M. Seymour and N. Provatas. Structural phase field crystal approach for modeling graphene and other twodimensional structures, Physical Review B, 2016, 93(3): 035447.

[10] V. Vítek, Intrinsic stacking faults in body-centred cubic crystals, Philosophical Magazine, 1968, 18(154):773-786.

[11] DAI Shuyang, XIANG Yang, D. J. Srolovitz. Structure and energy of (1 1 1) low-angle twist boundaries in Al, Cu and Ni, Acta materialia, 2013, 61(4):1327-1337.

[12] ZHOU Songsong, HAN Jian, DAI Shuyang, SUN Jianwei, D. J. Srolovitz. van der Waals bilayer energetics: Generalized stackingfault energy of graphene, boron nitride, and graphene/boron nitride bilayers, Physical Review B, 2015, 92(15): 155438.

[13] J. S. Alden, A. W. Tsen, P. Y. Huang, H. Robert, B. Lola, P. Jiwoong, D. A. Muller, and P. L. Mceuen, Strain solitons and topological defects in bilayer graphene, Proceedings of the National Academy of Sciences of the United States of America, 2013, 110(28): 11256-11260.